The interaction of dislocations and hydrogen-vacancy complexes and its importance for deformation-induced proto nano-voids formation in α-Fe

Suzhi Li[1,2,3], Yonggang Li[2,4], Yu-Chieh Lo[2], Thirumalai Neeraj[5*], Rajagopalan Srinivasan[5], Xiangdong Ding[1], Jun Sun[1], Liang Qi[2], Peter Gumbsch[3,6] and Ju Li[2*]

[1] *State Key Laboratory for Mechanical Behavior of Materials and Frontier Institute of Science and Technology, Xi'an Jiaotong University, Xi'an 710049, China*

[2] *Department of Nuclear Science and Engineering and Department of Materials Science and Engineering, Massachusetts Institute of Technology, Cambridge, Massachusetts 02139, USA*

[3] *Institute for Applied Materials, Karlsruhe Institute of Technology, Karlsruhe 76131, Germany*

[4] *Key Laboratory for Materials Physics, Institute of Solid State Physics, Chinese Academy of Sciences, Hefei, 230031, China*

[5] *Corporate Strategic Research, ExxonMobil Research and Engineering, Annandale, NJ 08801 USA*

[6] *Fraunhofer-Institut für Werkstoffmechanik IWM, Wöhlerstrasse 11, 79108 Freiburg, Germany*

*e-mail: neeraj.s.thirumalai@exxonmobil.com (T.N.)

liju@mit.edu (J.L.)

Abstract

By using multi-scale simulation techniques, we probed the role of hydrogen-vacancy complexes on nucleation and growth of proto nano-voids upon dislocation plasticity in α-Fe. Our atomistic simulations reveal that, unlike a lattice vacancy, a hydrogen-vacancy complex is not absorbed by dislocations sweeping through the lattice. Additionally, this complex has lower lattice diffusivity; therefore, it has a lower probability of encountering and being absorbed by various lattice sinks. Hence, it can exist metastably for a rather long time. Our large-scale atomistic simulations show that when metals undergo plastic deformation in the presence of hydrogen at low homologous temperatures, the mechanically driven out-of-equilibrium dislocation processes can produce extremely high concentrations of hydrogen-vacancy complex (10^{-5}~10^{-3}). Under such high concentrations, these complexes prefer to grow by absorbing additional vacancies and act as the embryos for the formation of proto nano-voids. The current work provides the possible route for the experimentally observed nano-void formation in the context of hydrogen-induced failure and also bridge the link from the atomic-scale events to the macroscopic failure.

Keywords: hydrogen-vacancy complexes; proto nano-voids; multi-scale modeling; hydrogen embrittlement

1. Introduction

Hydrogen embrittlement of metals is a major concern in many industries, ranging from oil and gas industry to off-shore wind turbines to hydrogen gas transport for a hydrogen economy (Gangloff and Somerday, 2012). Although several groups have proposed different models in the past, the mechanisms of hydrogen-induced failure are still not fully understood. Many studies have shown that H can enhance dislocation mobility; indeed, this led to the proposed hydrogen enhanced localized plasticity (HELP) mechanism of failure (Birnbaum and Sofronis, 1994; Robertson, 2001). However, there is still a large gap in the understanding of how dislocation slip in an atomic bond-switching manner can lead to fracture in a bond-breaking manner. Another mechanism that has been proposed is the hydrogen enhanced decohesion (HEDE) mechanism where it is proposed that local accumulation of H at crack tips can lead to weakening of bonds leading to fracture (Gerberich et al., 1991). It has been proposed that crack-tip dislocation activity leads to high stresses about 20 nm ahead of crack tip leading to accumulation of H of the order C_H ~ 0.5 leading to decohesion and failure (Gerberich et al., 1991). More recently, it was proposed that high H accumulation (C_H ~ $0.6-0.8$) at crack tips leads to suppression of dislocation emission from crack tip leading to brittle fracture (Song and Curtin, 2012). This proposal is inconsistent with the clear experimental evidence that there is significant plasticity associated with hydrogen embrittlement (Martin et al., 2011a; Martin et al., 2011b; Neeraj et al., 2012). It should be noted that in these proposals the local H content needs to be enhanced by several orders of magnitude with C_H approaching unity from very small initial concentrations of $C_H \sim 10^{-5}$ and thus appears to be physically unreasonable. Some other studies attributed the cause for embrittlement to H-enhanced Va generation and accumulation (Nagumo et al., 2001; Sakaki et al., 2006; Takai et al., 2008).

Our recent work showed the experimental evidence for nano-voiding along quasi-brittle fracture surfaces in hydrogen embrittled steels (Neeraj et al., 2012). It was proposed that plasticity-generated, hydrogen stabilized vacancy damage and vacancy aggregation were the primary cause for nano-voiding (Neeraj et al., 2012). However, there is still lack of atomic/microscopic level understanding on the formation of nano-voids from dislocation-hydrogen-vacancy interactions. The stabilization of vacancy by hydrogen is known to be in the form of hydrogen-vacancy complexes (VaH_n). The hydrogen-vacancy complexes have been studied previously using density functional theory (DFT) calculations (Lu and Kaxiras, 2005; Tateyama and Ohno, 2003). These calculations indicated that VaH_n complex had a good stability in different metals and might serve

as the embryos for void formation (Lu and Kaxiras, 2005). However, these calculations are limited to the study of energetics of hydrogen-vacancy complexes and cannot provide a possible route for how such complexes evolve to form voids in plastic deformation. In this paper, we probe the role of hydrogen-vacancy complexes on proto nano-voids formation in dislocation plasticity in α-Fe by using multi-scale simulation methods.

On the topic of deformation-induced voids, there were various works carried out to investigate the micro-void growth and material ductility. For example, several analytical models have been developed and extended to understand voids growth in alloys and steels (Benzerga et al., 2004; Fischer and Antretter, 2009; Khan and Liu, 2012; Lecarme et al., 2011; Li et al., 2011; Lou et al., 2014; Malcher et al., 2014; Tutyshkin et al., 2014). Besides experiments performed at microscopic level (Alinaghian et al., 2014; Tasan et al., 2014; Xu et al., 2015), some molecular dynamics simulations provided atomic view on growth of voids (Bringa et al., 2010; Traiviratana et al., 2008; Zhao et al., 2009). However, almost all these studies are focused on the hydrogen-free systems and most of the studies are on micro-void growth and coalescence. Here in the framework of hydrogen-induced failure, we find that hydrogen plays a significant role in the void formation. Our work shows that the hydrogen-vacancy complex plays an important role on proto nano-void nucleation and coalescence. This work attempts to bridge the link between the atomic-scale events of hydrogen-vacancy complexes and experimentally observed nano-voids formation microscopically.

2. Methodology

2.1. Molecular dynamics method

In this study, we use multi-scale simulations to study the properties of VaH_n complex and probe its role on proto nano-voids formation in α-Fe. We first performed the molecular dynamics (MD) simulations to study the basic properties of VaH_n complex, such as its stability, mobility and especially its interaction with dislocations. We then carried out large-scale MD calculations to study the generation and annihilation on plasticity of α-Fe under different H concentration. The atomic interaction in Fe-H system was described by an embedded atom method (EAM) potential (Ackland et al., 2004; Daw and Baskes, 1984; Ramasubramaniam et al., 2009). The deformation was performed at 300 K using a Nosé-Hoover thermostat (Hoover, 1985; Nose, 1984). The MD

calculations were carried out using the LAMMPS code (Plimpton, 1995) and the atomic configurations were visualized by AtomEye (Li, 2003).

In order to extract the vacancy information from MD simulations, we developed a "filling-in" method to determine Va position and its concentration based on crystallographic symmetry and energy minimization of the system. Figure 1 shows the searching procedure in a two-dimensional lattice grid schematically. For a perfect lattice structure, the atoms are placed right in the lattice sites (Fig. 1a). However, in reality, for a crystal upon deformation at 300 K, the atoms may have a slight deviation from the central position due to the thermal fluctuation or local distortion (Fig. 1b). The coordination number (CN) for each atom is still kept to be 4 if only the nearest-neighbor interaction is considered. Now suppose we have a small vacancy cluster containing four vacancies in the deformed crystal (Fig. 1c). The searching process will be carried out from the outer space to the inner space of the vacancy cluster. Due to the bond loss, the neighboring atoms around these vacancies will have a CN smaller than 4. We first search the atoms with one bond loss as CN = 3 (Fig. 1d). Then a virtual atom is filled in the potential vacancy site based on the crystal symmetry (Fig. 1e) as

$$\begin{cases} x_{virtual} = 4x_i - \sum_j x_j \\ y_{virtual} = 4y_i - \sum_j y_j \end{cases}, \qquad (1)$$

where (x_{virtual}, y_{virtual}) is the coordinate of virtual atom, (x_i, y_i) is the coordinate of searched atom with CN = 3, and (x_j, y_j) is the coordinate of neighbor atoms of atom *i*. However, the detected vacancy position is not very accurate due to the atom deviation mentioned above. After filling in, the virtual atom, energy minimization is performed according to the local potential field while keeping the position of other real atoms fixed. Then the position of virtual atom can be "corrected" to close to the vacancy position (Fig. 1f). After filling in, the coordination number of both real atoms and virtual atoms are updated (Fig. 1g). The searching continuous until there is no potential vacancy position available (Fig. 1h-i). The filled virtual atoms could be considered the vacancies we would like to detect. The flow chart for the searching process is shown in Fig. 1j. This method can be easily extended to three-dimensional system. By utilizing this "virtual atoms filling" method, the vacancy position and vacancy number (or concentration) could be determined accurately.

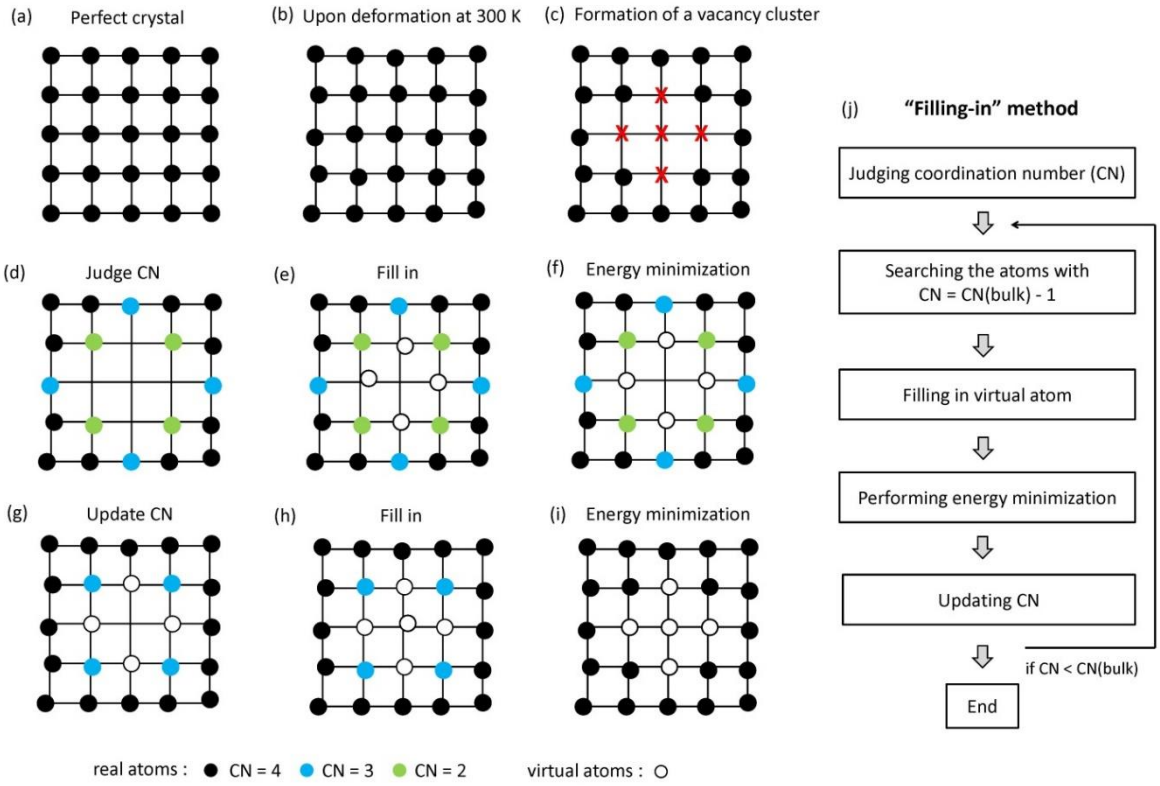

Fig. 1. Schematic illustration of "virtual atoms filling-in" method for searching vacancies in atomistic simulations.

2.2. Cluster dynamics method

Due to the limitation of short time period in MD simulations, a cluster dynamics (CD) model was developed to study the long-time evolution of the system based on the mean-field rate theory (Li et al., 2012) and grouping numerical method (Golubov et al., 2001). The evolution of clusters can be described by solving two-dimensional matter equation (ME) as

$$\mathrm{d}C(x,y,t)/\mathrm{d}t = [J_x(x\text{-}1,y,t) - J_x(x,y,t)] + [J_y(x,y\text{-}1,t) - J_y(x,y,t)] \ , \tag{2}$$

with the fluxes $J_x(x, y, t)$ and $J_y(x, y, t)$ calculated as

$$\begin{cases} J_x(x,y,t) = P_x(x,y,t)C(x,y,t) - Q_x(x{+}1,y,t)C(x,y,t) \\ J_y(x,y,t) = P_y(x,y,t)C(x,y,t) - Q_x(x,y{+}1,t)C(x,y,t) \end{cases}, \tag{3}$$

where *x* and *y* are related to a number of vacancies and H atoms in a particular cluster, respectively, the coefficients $P_x(x,y,t)$, $P_y(x,y,t)$, $Q_x(x,y,t)$, $Q_y(x,y,t)$ are the rates of capture/evaporation reactions between the monomers and clusters leading to a change in the cluster size *x* and *y*, respectively, which can be obtained from different experimental and theoretical parameters.

With the grouping method (Golubov et al., 2001), the clusters are grouped within of a group of widths $\Delta x_i = x_i - x_{i-1}$ and $\Delta y_j = y_j - y_{j-1}$ which include the clusters of the sizes,

$$\begin{cases} x = x_{i-1} + m, \ (m = 1, ..., \Delta x_i) \\ y = y_{j-1} + n, \ (n = 1, ..., \Delta y_j) \end{cases}, \tag{4}$$

respectively, where the subscript *i* and *j* indicate the numbers of a group in *x*- and *y*-spaces, respectively. Thus each group consists of $l_{i,j} = \Delta x_i \Delta y_j$ numbers of clusters of different sizes and is defined by the double index "*i*,*j*".

Approximate the size-distribution function (SDF), $C(x,y,t)$, by a linear function within a group *i*,*j* of the type,

$$C_{i,j}(x,y) = L_0^{i,j} + L_{1x}^{i,j}(x - \langle x \rangle_i) + L_{1y}^{i,j}(y - \langle y \rangle_j). \tag{5}$$

By assuming that all capture/evaporation efficiencies, $P_x(x,y,t)$, $P_y(x,y,t)$, $Q_x(x,y,t)$ and $Q_y(x,y,t)$, are equal within a group (Kiritani, 1973) and taking into account that SDF within a group is linear depends on *x* and *y*, the coefficients $L_0^{i,j}, L_{1x}^{i,j}, L_{1y}^{i,j}$ can be finally presented in the following form,

$$\frac{dL_0^{i,j}}{dt} = \frac{1}{\Delta x_i}[J_x(x_{i-1}, \langle y \rangle_j) - J_x(x_i, \langle y \rangle_j)] + \frac{1}{\Delta y_j}[J_y(\langle x \rangle_i, y_{j-1}) - J_y(\langle x \rangle_i, y_j)]. \tag{6}$$

$$\begin{aligned} \frac{dL_{1x}^{i,j}}{dt} = &-\frac{\Delta x_i - 1}{2\sigma_i^{\,2}\Delta x_i}[J_x(x_{i-1}, \langle y \rangle_j) + J_x(x_i, \langle y \rangle_j) - 2J_x(\langle x \rangle_i - \frac{1}{2}, \langle y \rangle_j)] \\ &+ \frac{1}{\Delta y_j}\{[J_y(\langle x \rangle_i + 1, y_{j-1}) - J_y(\langle x \rangle_i, y_{j-1})] - [J_y(\langle x \rangle_i + 1, y_j) - J_y(\langle x \rangle_i, y_j)]\} \end{aligned}. \tag{7}$$

$$\frac{dL_{1y}^{i,j}}{dt} = -\frac{\Delta y_j - 1}{2\sigma_j{}^2 \Delta y_j}[J_y(\langle x\rangle_i, y_{j-1}) + J_y(\langle x\rangle_i, y_j) - 2J_y(\langle x\rangle_i, \langle y\rangle_j - \frac{1}{2})] + \frac{1}{\Delta x_i}\{[J_x(x_{i-1}, \langle y\rangle_j + 1) - J_x(x_{i-1}, \langle y\rangle_j)] - [J_x(x_i, \langle y\rangle_j + 1) - J_y(x_i, \langle y\rangle_j)]\} \quad (8)$$

where, $\langle x\rangle_i$ and $\langle y\rangle_j$ are the mean sizes of clusters, σ_i^2 and σ_j^2 are dispersions of cluster sizes within an *i*,*j* group, respectively; $\langle J_x\rangle^*_{i,j(n)}$ and $\langle J_y\rangle^*_{i(m),j}$ are the mean flux J_x inside *i*,*j*-th group at a given size of y ($y = y_{j-1} + n$) and the mean flux J_y inside *i*,*j*-th group at a given size of x ($x = x_{i-1} + m$), respectively. Thus instead of solving $l_{i,j} = \Delta x_i \Delta y_j$ numbers of MEs for the group it is necessary to solve the three equations only.

The detailed description of model setup and parameters for each technique are shown in the corresponding section below.

3. Results and Discussion

3.1. MD simulations on the basic properties of hydrogen-vacancy complexes

In bulk α-Fe, H atoms prefer to dissolve in tetrahedral (T) interstitial sites than octahedral (O) sites. The dissolution energy (E_d) of H in bulk T-site is defined as

$$E_d = E(\mathrm{Fe}_N\mathrm{H}) - E(\mathrm{Fe}_N) - E(\mathrm{H}_2)/2, \quad (9)$$

where the function E is the cohesive energy of supercell. $\mathrm{Fe}_N\mathrm{H}$ is the perfect Fe supercell with one H atom in bulk T-site, Fe_N is the perfect Fe supercell with N as the total number of Fe atoms in the supercell, and H_2 is the hydrogen molecular. The binding energy of H_2 is -2.37 eV per atom. The current potential can produce the dissolution energy around 0.30 eV for H in bulk T-site, which is consistent with the experimental measurement (Hirth, 1980) and first-principle calculations (Tateyama and Ohno, 2003).

Many first-principle calculations have shown that multiple H atoms can bond to Va in perfect crystals as $\mathrm{Va} + n\mathrm{H} \rightarrow \mathrm{VaH}_n$ (Hayward and Deo, 2011; Lu and Kaxiras, 2005; Tateyama and Ohno, 2003). The product is a relatively stable complex. Once hydrogen-vacancy complexes are formed during mechanical deformation, they would inevitably interact with dislocations. Thus, it is very important to know how they behave when meeting with dislocations. In this section, by

using MD simulations, we first studied the energetics of hydrogen-vacancy complexes in α-Fe. Then we probed the interactions of dislocation with Va, VaH and H by studying four independent events. The mobility of VaH was then investigated and compared to that of Va. We develop an overall understanding on the basic properties of hydrogen-vacancy complex based on these studies.

3.1.1 Stability of the hydrogen-vacancy complexes

More recently, several groups have utilized atomistic modeling to study the energetics of hydrogen-vacancy complexes in α-Fe (Hayward and Deo, 2011; Hayward and Fu, 2013; Tateyama and Ohno, 2003). The density functional theory (DFT) calculations show that vacancies can be stabilized by H as H lowers both the vacancy formation energy and also bind strongly with vacancies to form the VaH_n complexes (Hayward and Fu, 2013; Tateyama and Ohno, 2003). The results show that one Va can trap up to six H and VaH_2 is the major complex (Tateyama and Ohno, 2003). It also indicates that the hydrogen-vacancy complexes would prefer to form spherical clusters as against planar or cylindrical clusters along <111> (Hayward and Fu, 2013; Tateyama and Ohno, 2003). Moreover, the VaH_n complexes also widely exist in other fcc and bcc metals (Lu and Kaxiras, 2005; Ohsawa et al., 2012).

In order to test the present EAM potential for its capability to correctly predict the energetics of hydrogen-vacancy complex, we also calculated the binding energy of VaH_n (n = 1−6) complex. The averaged binding energy of the VaH_n complexes is defined as

$$E_b(VaH_n) = [E(Fe_NH) - E(Fe_N)] - [E(Fe_{N-1}H_n) - E(Fe_{N-1}H_{n-1})], \quad (10)$$

where the function E is the cohesive energy of supercell (Nagumo et al., 2001; Ohsawa et al., 2012). Fe_NH is the perfect Fe supercell with one H atom in bulk interstitial site, Fe_N is the perfect Fe supercell and N is the total number of Fe atoms in the supercell. $Fe_{N-1}H_n$ and $Fe_{N-1}H_{n-1}$ refers to a supercell containing the VaH_n complex and VaH_{n-1} complex, respectively. Table 1 shows the averaged binding energy of multiple H atoms around a Va. The data we obtained here shows the same trend and are comparable to those obtained by first-principle calculations (Tateyama and Ohno, 2003). Therefore, the current EAM potential can represent the energetics of VaH_n complex well.

Table 1 Averaged binding energy of VaH_n (n = 1−6) in α-Fe. The units are in eV.

	VaH	VaH_2	VaH_3	VaH_4	VaH_5	VaH_6
MD (current work)	0.603	0.603	0.425	0.346	0.217	0.158
DFT (Tateyama and Ohno, 2003)	0.559	0.612	0.399	0.276	0.335	-0.019

3.1.2. Interactions of dislocation with hydrogen-vacancy complexes

We have shown that hydrogen-vacancy complex can exit stably in crystals. However, little is known about its stability when interacting with dislocations. In the following, we study its interaction with dislocations and reveal the difference of VaH_n complex and Va in response to dislocations by investigating four independent events. As shown in Fig. 2, we first created the $a/2$<111>-type edge dislocation with a length of 12 nm. The simulation box was oriented along x-[111], y-[$\bar{1}$01], z-[1$\bar{2}$1]. Then we applied shear strain in the xz-plane to drive dislocation glide along x direction. Different types of point defects (H, Va and VaH) were placed in the glide plane to study their interactions with edge dislocations.

In our simulations, it is first shown that unlike an isolated Va, a VaH complex exhibits good stability when colliding with edge dislocations during plastic deformation. Figure 2a and 2b compare the different responses of Va and VaH when a $a/2$<111>-type edge dislocation hits them head-on in α-Fe. An un-hydrogenated Va is not stable when meeting an edge dislocation and is absorbed by the dislocation, forming a Va jog on the dislocation line (Fig. 2a). After absorbing the Va, the dislocation still has sufficient mobility for further glide, carrying the mass deficiency with it. In contrast, since the VaH complex is quite stable, annihilation by dislocation absorption is not observed when an edge dislocation hits a VaH. This indicates that the sink role of an edge dislocation is lost (Fig. 2b). The VaH stability can be further demonstrated in the competition for Va absorption between lattice H and an edge dislocation. As shown in Fig. 2c, although an edge dislocation can absorb an isolated Va and carry it along (Fig. 2a), the lattice H can "grab" this absorbed Va from the moving dislocation, thus forming a stationary VaH detached from the dislocation. Moreover, VaH can grow further by trapping more vacancies that were absorbed as Va jogs in dislocations (Fig. 2d). We characterize this type of growth of the hydrogen-vacancy

complex as *displacive growth*, since dislocations bring in the mass deficiency to the site of growth by (displacive) glide. This is distinct from the typical diffusive growth that occurs by Va diffusion. This also illustrates the unexpected role played by gliding edge dislocations as Va transporters that help further Va accumulation at the VaH_n complexes.

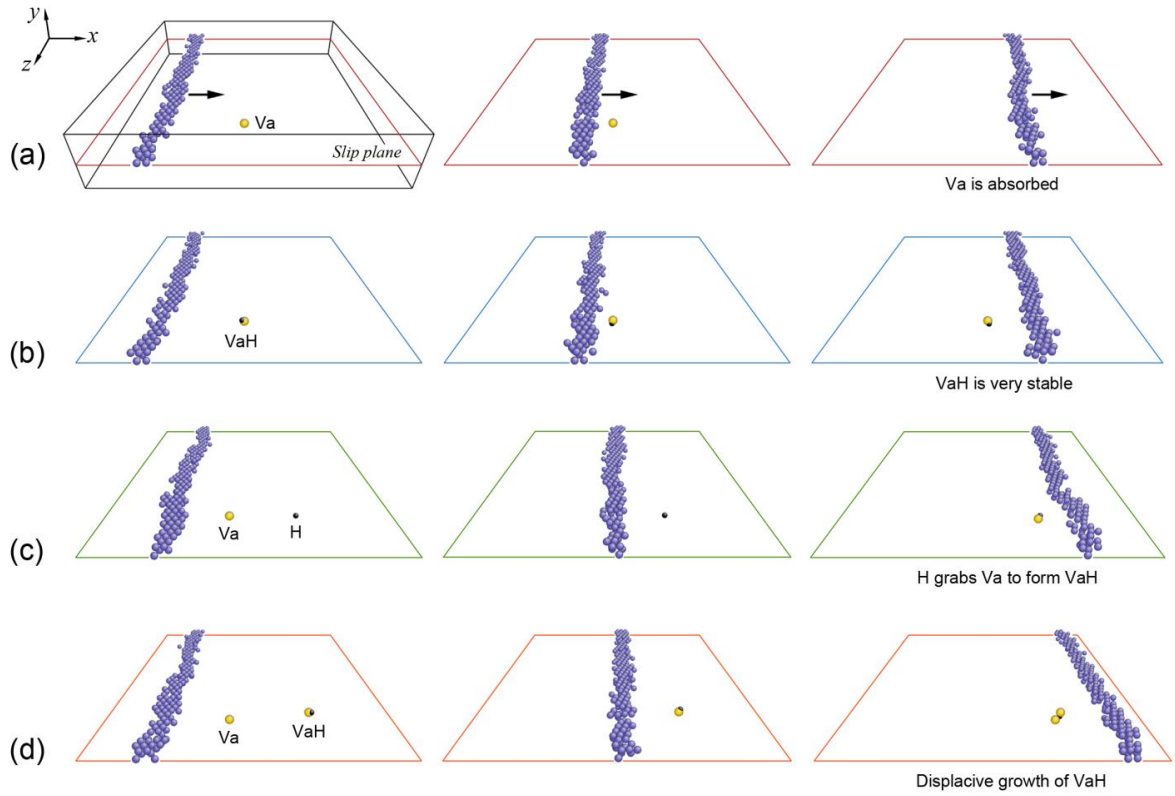

Fig. 2. Four independent events illustrating the high stability of hydrogen-vacancy complex when interacting with dislocations in α-Fe. Crystals are oriented along *x*-[111], *y*-[$\bar{1}$01], *z*-[1$\bar{2}$1]. Spheres with slate blue, gold and black colors refer to iron atoms in dislocations, vacancies and hydrogen, respectively. The radius of vacancy and hydrogen are enlarged for clarity. (a) When a *a*/2<111>-type edge dislocation interacts with a vacancy in the slip plane, the dislocation absorbs the vacancy. (b) In contrast, the hydrogen-vacancy complex is very stable when colliding with an edge dislocation. (c) The stability of hydrogen-vacancy complex is further confirmed when lattice hydrogen grabs an absorbed vacancy from an edge dislocation and stabilize it in the form of a hydrogen-vacancy complex. (d) The hydrogen-vacancy complex can even grow displacively by capturing more vacancies that were absorbed by edge dislocations.

3.1.3. Migration barriers of Va, VaH and H

Even though the hydrogen-vacancy complex is stable when interacting with an edge dislocation sink in comparison to a vacancy, there is still the probability for it to annihilate to other sinks. In

reality, besides the mobile Va sinks such as edge dislocations, there are also immobile sinks in materials for vacancies and hydrogen-vacancy complexes such as prismatic loops, precipitates, grain boundaries, etc. Thus, there is a finite lifetime for hydrogen-vacancy complexes and vacancies before diffusing to these sinks and annihilating. We show below that a VaH not only has good stability, but also exhibits lower diffusivity as compared to a Va. Figure 3 compares the migration (diffusion) paths of VaH, Va and H calculated using the climbing image nudged elastic band (CINEB) method (Henkelman et al., 2000). In comparison to an activation barrier of 0.64 eV (E^m_{Va}) for Va diffusion, a VaH needs to overcome a higher barrier of 0.76 eV (E^m_{VaH}). Based on these activation barriers, a simple calculation of diffusion length L for a given time t can be calculated as

$$L = \sqrt{4Dt}, \tag{11}$$

with diffusion coefficient

$$D = D_0 \exp(-E^m / k_{\mathrm{B}} T), \tag{12}$$

where D_0 is pre-exponent coefficient, E^m is the diffusion barrier discussed above, k_{B} is the Boltzmann constant and T is absolute temperature]. By setting diffusion length L equal to an average sink length L_{sink}, we can obtain the lifetime for these defects as $t_{\mathrm{life}} = {L_{\mathrm{sink}}}^2 / 4D$. Assuming a sink length of L_{sink} = 100 nm, D_0 = 2.76 cm^2/s (Iijima et al., 1988) and T = 300 K, a Va can have a lifetime of around 0.5 second. In comparison, a VaH can have a much longer lifetime (~50 s) that is two orders of magnitude larger than that of Va. In addition, there is also the possibility of VaH_n complex dissociation into lattice H and Va ($\mathrm{VaH}_n \rightarrow \mathrm{Va} + n\mathrm{H}$). The energy barrier for one H atom escaping from VaH is around 0.54 eV. Thus, the hydrogen-vacancy complex is estimated to move slowly under the condition of high H concentration because the released Va can be re-stabilized by H before diffusing large distances when considering the very high diffusivity of H (E^m_{H} = 0.04 eV).

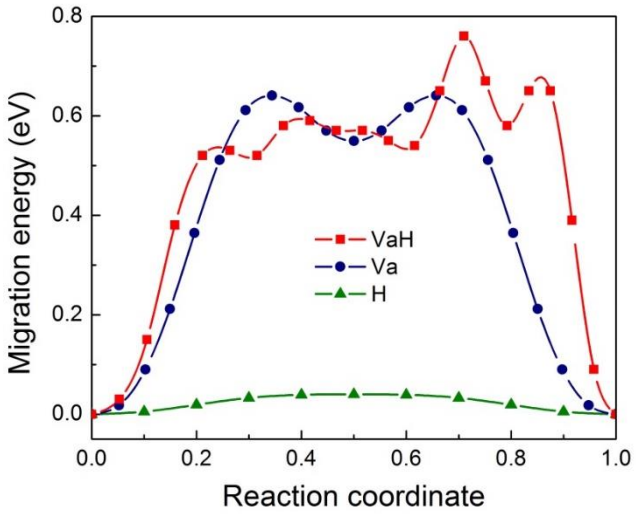

Fig. 3. Migration paths of hydrogen-vacancy complex, vacancy and hydrogen in α-Fe. As indicated in red, blue and green lines, the migration barriers of corresponding point defects are 0.76 eV, 0.64 eV and 0.04 eV, respectively.

3.2. Evolution of hydrogen-vacancy complexes during plastic deformation

We have shown that the hydrogen-vacancy complex has a good stability and relatively low diffusivity. Next we studied the generation and annihilation of VaH_n complexes during plastic deformation and probed its influence on mechanical performance by using large-scale MD simulations. We conducted uniaxial tension tests in α-Fe at 300 K under different H concentrations (C_H). The variation of VaH_n complex concentration (C_{VaH_n}) with different C_H was further obtained and analyzed. Moreover, a model for describing the relationship of VaH_n complex concentration and strain was constructed to support our simulation results.

3.2.1. Generation and annihilation of hydrogen-vacancy complexes in dislocation plasticity by large-scale MD simulations

Figure 4 illustrates the complete sequence of model creation and sample deformation for large-scale MD simulation schematically. We first constructed dislocation configurations in a defect-free crystal. The sample sizes approached 23 nm × 23 nm × 23 nm (containing more than one million atoms) with periodic boundary conditions in three directions. To make our results more general, two models with completely different starting configurations of dislocations were created. Model (a) contained four symmetrically-distributed *a*/2<111> prismatic loops (PLs) with tensile

axis along *x*-[100], and model (b) had four *a*/2<111>/{110} shear loops (SLs) along *x*-[011]. We find that PLs could exist stably in a small radius of several nanometers in stress-free state, as illustrated in Fig. 5a. This stable configuration was taken as the initial configuration for subsequent tensile deformation. However, SLs were not stable in stress-free state under such small radius due to the large dislocation line tension of $Gb/2r$, where G is shear modulus, b is Burgers vector and r is loop radius (Hirth and Lothe, 1992). After being created, they tend to shrink and annihilate driven by minimization of elastic energy. In our present simulation, in order to obtain a stable dislocation configuration originated from SLs, we first applied certain amount of pre-stress to the system below the elastic limit. Then we applied relative displacement between two neighboring atomic planes to induce dislocation loops while holding the pre-stress. After the loops were created, they did not shrink but expanded freely and finally evolved to a stable dislocation network. We finally released the stress to make the system go back to a stress-free state. This stable configuration was taken as the initial configuration for our large-scale MD simulations. The complete generation of starting configuration is shown in Fig. 5b. After dislocations were created, H was added and randomly distributed to each system with C_H ranging from 10^{-4} to 10^{-2} in atomic ratio. In experimental studies, the net H content in iron or steels is typically quite low and is on the order of 10^{-5}~10^{-3} in atomic ratio (Nagumo et al., 2001; Takai et al., 2008). However, H-induced failure usually occurs at sites of high local stresses such as a crack tip, where C_H can be orders of magnitude larger than the average value (Johnson et al., 1958; Sofronis and McMeeking, 1989; Troiano, 1960). In our MD simulations we set C_H ranging from 10^{-4}~10^{-2} in atomic concentration (corresponding to 2~200 ppm in weight concentration) to cover this range reasonably. After relaxation for several nanoseconds, a maximum strain of 60% was applied under a strain rate of 10^9 s^{-1}.

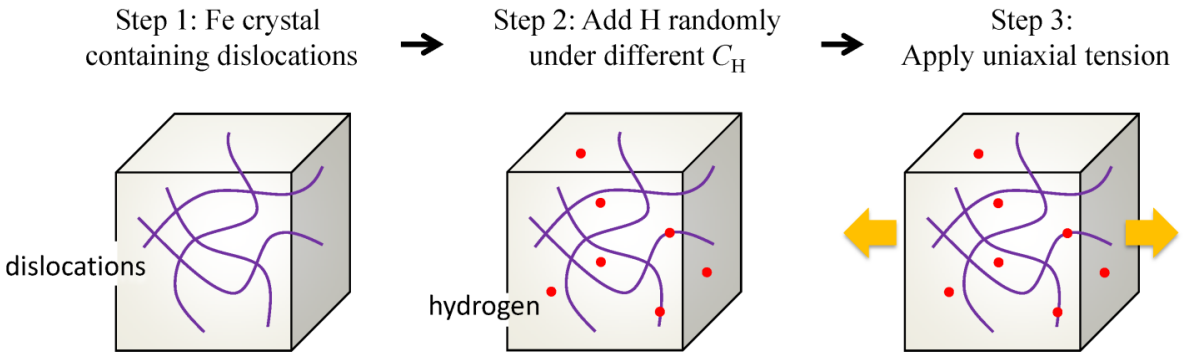

Fig. 4. Illustration of model creation and sample deformation in large-scale MD simulations schematically. The purple curves represent dislocation lines and the red spots refer to hydrogen atoms.

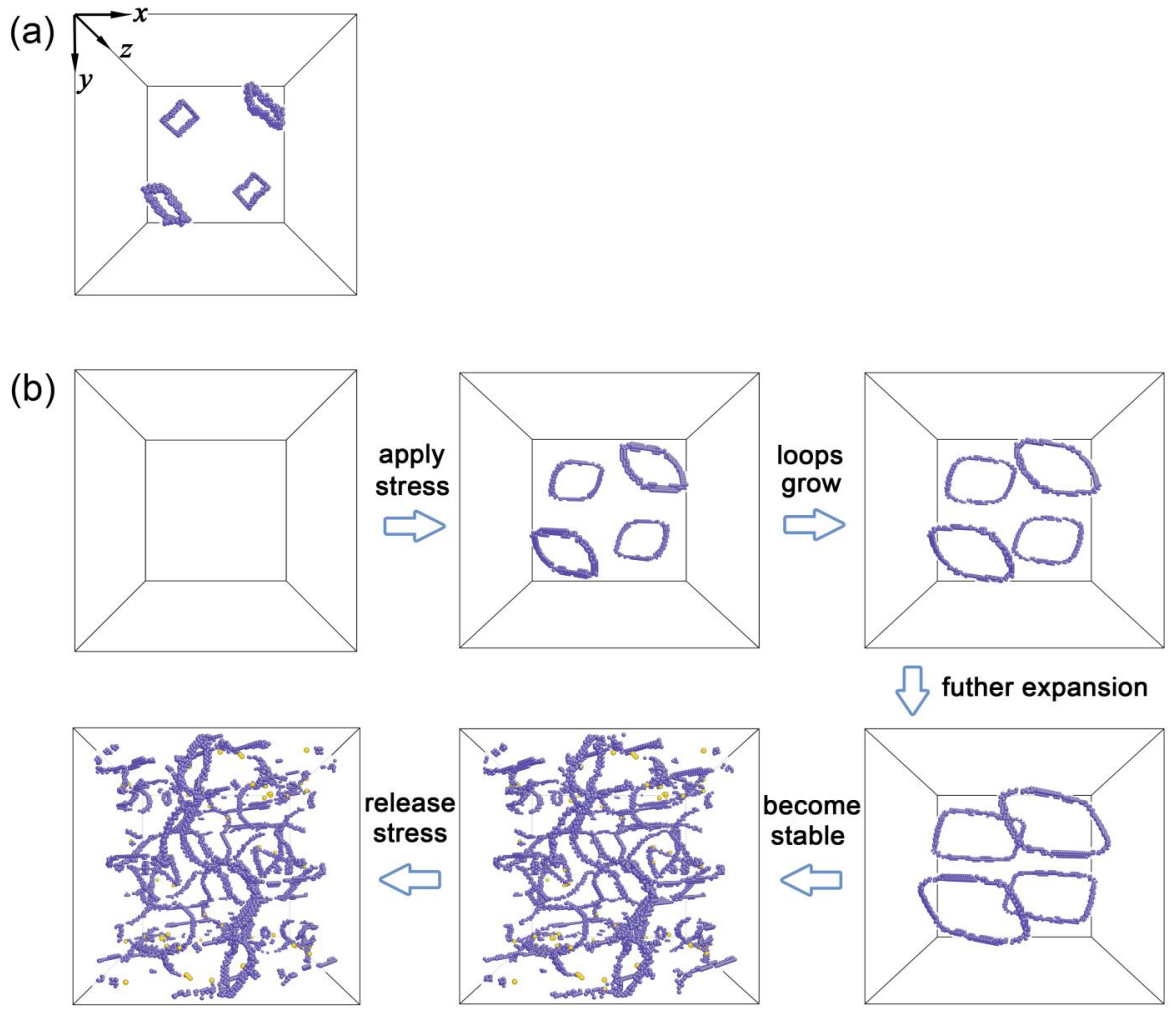

Fig. 5. Stable dislocation configurations (a) prismatic loops (PLs) and (b) shear loops (SLs). Spheres with slate blue and gold color refer to the iron atoms in dislocations and vacancies respectively. PLs are stable when created in a stress-free state while SLs were not. In order to create a stable configuration originated from shear loops, a pre-stress within the elastic limit was first applied to the perfect crystal. Then four $a/2\langle 111\rangle/\{110\}$ shear loops were created by moving two rigid atomic planes. The newly created loops then expanded and interacted with each other to form a stable dislocation network. The pre-stress was then released and this final configuration was taken as the initial state for uniaxial tension simulations in our manuscript.

In the simulations, we find that dislocations can act as both the sources for vacancies generation and sinks for vacancies absorption. A large amount of non-equilibrium (excess) vacancies were generated by dislocation plasticity consistent with experiments (Sakaki et al., 2006). During

dislocation plasticity Va generation typically came from four major dislocation processes (Hirth and Lothe, 1992) namely, (a) growth of prismatic loops, (b) non-conserved jog dragging, (c) cross-slip of screw dislocations, and (d) breaking of dislocation junctions. The spatial distribution of vacancies generated by each of the above dislocation processes has its own distinct characteristics. Therefore, the vacancies can correspondingly form either in a random or in an orderly (e.g. jog dragging) fashion, individually or collectively in space (see Supplementary Movies). In addition, the edge dislocations can also act as strong sinks for vacancies (see Fig. 2a). Therefore, a small group of vacancies will also annihilate when meeting the dislocation sinks.

In the presence of H, one can expect that a certain amount of these vacancies will transform into hydrogen-vacancy complexes by combining with H. However, as discussed above, the role of dislocations as strong sinks was greatly diminished in the presence of hydrogen-vacancy complexes. Those vacancies that are combined with H will be preserved during further dislocation interactions. Even once the vacancies are absorbed by edge dislocation sinks, we may expect that vacancy can diffuse easily along dislocation line (Lau et al., 2009). Since H atoms also prefer to accumulate along dislocations, the dislocation lines can provide a channel for vacancies to meet H quickly with the help of pipe diffusion. This might provide an additional pathway for forming VaH_n complexes. In essence, the presence of H biases the role of dislocation plasticity towards production or the role of a "source".

Figure 6a shows the variation in total concentration of vacancy and hydrogen-vacancy complex, C_V ($\equiv C_{Va} + C_{VaH_n}$), with applied strain ($\varepsilon$) under different C_H. These results were from the model system containing shear loops as the starting dislocation configuration and were taken as a typical example of the behavior. Note that all the concentrations (C_H, C_{Va}, C_{VaH_n}, C_V) shown here are in the unit of atomic ratio. We find that C_V can reach the order of 10^{-3} due to dislocation plasticity. The concentration of lattice vacancies shows a nearly linear increase when C_H (= 10^{-2}) is larger than C_V, while the linear increase is replaced by exponential saturation when C_H (= 10^{-4}~10^{-3}) approaches or is smaller than C_V. The differences in the response of C_V to C_H lie in the magnitude of hydrogen-vacancy complex concentration in system. As illustrated in Fig. 6b, for the condition of $C_H > C_V$, the magnitude of C_{VaH_n} can reach the same order as C_V. Thus it indicates that the majority of deformation-induced vacancies are stabilized as hydrogen-vacancy complexes and the sink role of edge dislocations is greatly weakened. However, as C_H is lowered, most of the vacancies are un-hydrogenated and can be absorbed by edge dislocation sinks easily (see Fig. 2a). Thus, the generation of vacancies by dislocation plasticity competes with annihilation due to

absorption at sinks. C_V goes to a lower steady-state value due to the balance between Va production and annihilation.

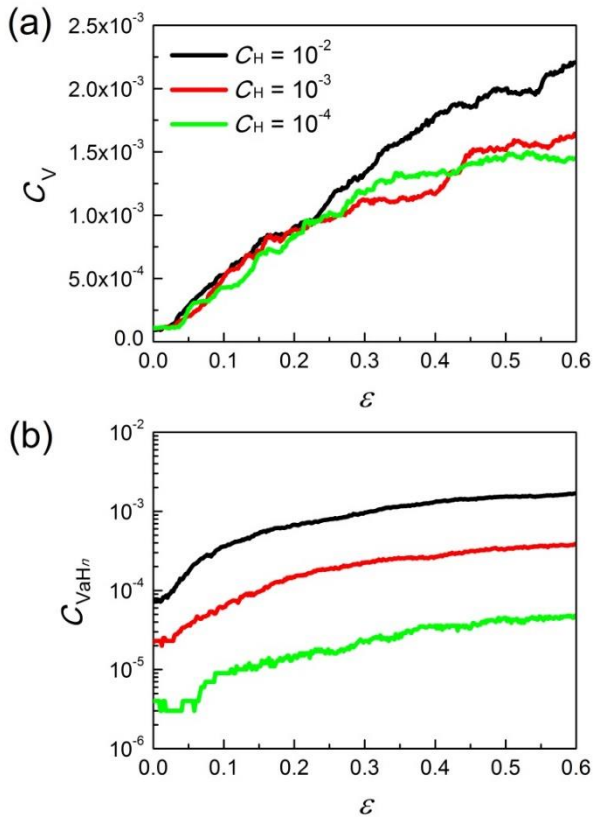

Fig. 6. Variation of (a) concentration of total vacancies and hydrogen-vacancy complexes (C_V) and (b) concentration of hydrogen-vacancy complexes (C_{VaH_n}) with applied strain (ε) under different hydrogen concentration (C_H) in iron. The total vacancies include both isolated vacancies and hydrogen-vacancy complexes. C_V, C_{VaH_n} and C_H are in the units of atomic ratio.

3.2.2. Model for describing the generation of vacancies and hydrogen-vacancy complexes

Figure 6a above shows a linear-increase of C_V with ε under $C_H = 10^{-2}$. Here we present a model to explain this linear relationship between C_V and ε. The net rate of C_V is given by

$$dC_V/dt = \Pi - \eta, \quad (13)$$

where Π and η are the production rate and annihilation rate of vacancies respectively (Militzer et al., 1994). In the absence of H, solving this equation will firstly show an exponential increase in Va concentration and finally approach a saturated value. However, under the condition of $C_H >$

C_V, the majority of generated vacancies are stabilized by H to form VaH_n complexes and they do not annihilate easily to sinks, so η will approach zero as a simple approximation. Hence we have the new dynamic equation for C_V under a higher H concentration as

$$dC_V/dt = \Pi. \quad (14)$$

The primary contribution to Π is calculated as

$$\Pi = \chi\Omega_0\sigma\dot{\varepsilon}/Q_f \text{ (Militzer et al., 1994)}, \quad (15)$$

where χ is a dimensionless constant, σ is flow stress, $\dot{\varepsilon}$ is strain rate, Ω_0 (= 1.18×10^{-29} m^3) is atomic volume and Q_f (= 1.53 eV) is Va formation energy. The coefficient χ represents the fraction of mechanical work of the applied stress stored in the vacancies generation. The magnitude of χ approaches 0.1 at elevated temperature near $0.5T_m$, where T_m is the melting point (Mecking and Estrin, 1980). Further, we know that $\sigma \sim \sqrt{\rho}$ (Taylor, 1934, 1938) and $\dot{\varepsilon} \sim \rho$, where ρ is dislocation density. Obviously, it indicates that vacancy generation rate is strongly dependent on dislocation density.

By integrating this equation, we obtain linear correlation between C_V and ε as

$$C_V = K\varepsilon + C_0, \quad (16)$$

where K is coefficient and C_0 is the initial concentration. The slope K then should be a function of stress σ as

$$K(\sigma) = \chi\Omega_0\sigma/Q_f. \quad (17)$$

We find that the magnitude of C_V under $C_H = 10^{-2}$ in our MD simulations is comparable to that predicted by this model. The flow stress for dislocation models (a) and (b) is 2.44 GPa and 3.14 GPa in our simulations, as shown in stress-strain curves in Fig. 7a. The slope of $K(\sigma)$ in our MD simulation are 3.93×10^{-3} and 3.50×10^{-3} by taking the linear fit of the data in strain range 0.06~0.6, as shown in Fig. 7b. The values predicated by the model above under such flow stress are 11.76×10^{-3} and 20.24×10^{-3}, respectively, several times larger than that in MD simulations. The deviation is due to overestimation of χ in the models (Mecking and Estrin, 1980), which is 0.1 at elevated temperature but should be smaller at 300 K here.

Based on our model above, we can manifest that our MD simulation can produce a good description of the variation of C_V with ε. As we shown above, the annihilation rate of Va is very

small when H concentration is large enough. Thus, the ratio of C_V/ε upon $C_H = 10^{-2}$ here could represent the vacancy generation ability during dislocation plasticity approximately. Figure 7b shows that the magnitude of C_V/ε is on the order of 10^{-3} in α-Fe. Correspondingly, when the system reaches a steady state, we can further expect the ratio of vacancy generation rate ($\dot{C}_V$) to strain rate ($\dot{\varepsilon}$) to be $\dot{C}_V/\dot{\varepsilon} \sim 10^{-3}$ approximately.

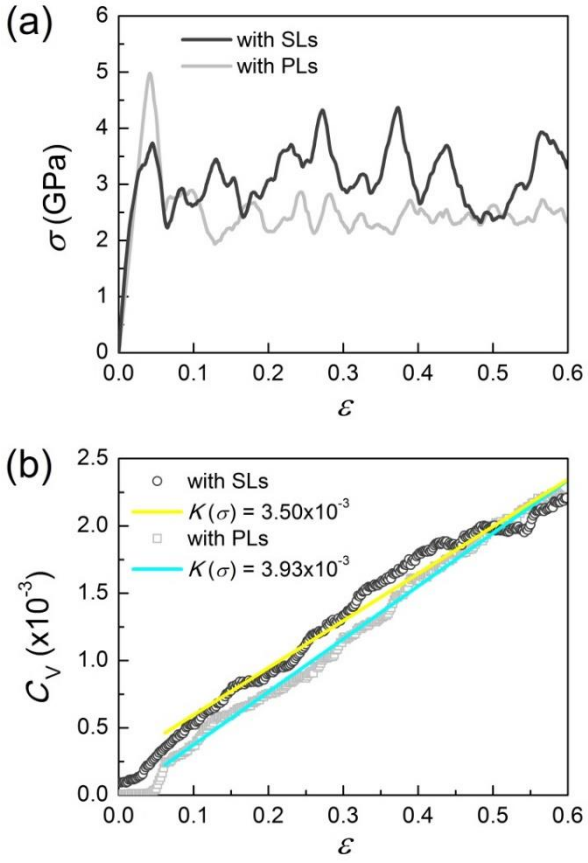

Fig. 7. (a) Stress-strain curve of uniaxial tension for both systems containing SLs and PLs under $C_H = 10^{-2}$, (b) Variation of concentration of total vacancies and hydrogen-vacancy complexes C_V ($\equiv C_{Va} + C_{VaH_n}$), including both unhydrogenated vacancies and hydrogen-vacancy complexes. The yellow and cyan solid lines are the linear fit to the two curves in strain range 0.06~0.6.

3.3. Probing the role of hydrogen-vacancy complexes on formation of proto nano-voids

It is well-known that the equilibrium concentration of vacancies is quite low in pure metals around room temperature. The vacancy concentration, C_{Va} only reaches of the order of 10^{-4}~10^{-3} when approaching the melting point (Kraftmakher, 1998). Here our simulations have shown that C_V can

be strongly out of thermal equilibrium due to dislocation plasticity in the presence of H. As mechanical energy is pumped into the system during deformation, the sluggish kinetics of VaH_n complex migration makes the system highly metastable, with C_V increasing equivalent to equilibrium concentrations near the melting point. Thus, C_V will reach a significantly high value ~10^3. It should be re-emphasized that such a vacancy-supersaturated state can only be obtained in the presence of H. For the system without H, the concentration of deformation-induced vacancies tends to go to equilibrium concentration by long-range diffusion (Fischer et al., 2011) due to their facile motion and lack of stabilization by H.

Next, we showed that the accumulation of excess vacancies and hydrogen-vacancy complexes could have significant effects on the mechanical properties of materials. As mentioned above, a mono-vacancy can be considered the smallest carrier of microstructural damage or the basic unit of "free volume". In many materials, mechanical performance will be degraded when the system sustains a high-density of free volume, such as during creep at elevated temperature (Hirth and Lothe, 1992), void swelling under irradiation (Brailsford and Bullough, 1972) and structure evolution under severe deformation (Valiev et al., 1996; Zehetbauer, 1993). As discussed next, the supersaturated vacancies formed in our system will also have a severe effect on the mechanical properties. In the discussion above we investigated deformation-induced free volume evolution during plasticity of Fe in the presence of H using MD methods. Due to the well-known timescale limitation of MD simulations, the time span of MD trajectory is constrained to be on the order of nanoseconds. Thus, those events (e.g., Va migration) that need a longer time to be activated (of the order of microseconds) cannot be captured well in MD simulations. To further probe the role of VaH_n complexes on nano-void nucleation and growth at reasonable timescales, we developed the coarse-grained cluster dynamics (CD) model to study long-time evolution of vacancies and VaH_n complexes.

The calculation parameters were set based on typical experimental conditions (Takai et al., 2008). Initial conditions were set as H concentration $C_H = 10^{-4}$, Va concentration $C_{Va} = 10^{-6}$, dislocation density $\rho = 10^{12}$ m^{-2}, average grain radius d = 10 μm, temperature T = 300 K, strain rate $\dot{\varepsilon} = 10^{-2}$ s^{-1}. As we show above, our MD simulations provided a good description of $\dot{C}_V/\dot{\varepsilon} \sim 10^{-3}$. Thus, the magnitude of $\dot{C}_{Va}$ would be 10^{-5} s^{-1} following the above relationship. All the other key parameters are shown in Table 2.

Table 2 Physical parameters used for the CD modeling of α-Fe.

Parameters	Symbol	Value
Temperature	T	300 K
Lattice constant	a	0.28553 nm
Initial H concentration (Takai et al., 2008)	C_{H}^{0}	10^{-4} (atomic ratio)
Initial Va concentration (this paper)	C_{Va}^{0}	10^{-6} (atomic ratio)
Va generation rate (this paper)	$\dot{C}_{\mathrm{Va}}$	10^{-5} /atom/s
Dislocation line density (Meslin et al., 2008)	ρ	10^{12} m^{-2}
Grain size (this paper)	d	10 μm
Va pre-exponential factor (Hardouin Duparc et al., 2002)	D_{Va}^{0}	~10^{-4} m^2/s
H pre-exponential factor (this paper)	D_{H}^{0}	~10^{-7} m^2/s
Capture efficiency of Va by dislocations (Etienne et al., 2010; Fu et al., 2005; Hardouin Duparc et al., 2002)	$Z_{\mathrm{Va}}^{\mathrm{D}}$	1.0
Capture efficiency of H by dislocations (this paper)	$Z_{\mathrm{H}}^{\mathrm{D}}$	1.0
H solution energy (Tateyama and Ohno, 2003)	E_{H}^{s}	0.29 eV
H migration energy (Ramasubramaniam et al., 2009)	E_{H}^{m}	0.04 eV
Va formation energy (this paper)	E_{Va}^{f}	1.53 eV
Va migration energy (this paper)	E_{Va}^{m}	0.64 eV
Va-Va binding energy (Tateyama and Ohno, 2003)	$E_{\mathrm{Va\text{-}Va}}^{b}$	0.21 eV
Binding energy of H in edge dislocation (Kimizuka and Ogata, 2011)	$E_{\mathrm{D\text{-}H}}^{b}$	0.61 eV
Binding energies of Va/H with $\mathrm{Va}_m\mathrm{H}_n$ clusters (Hayward and Deo, 2011; Liu et al., 2009)	$E_{\mathrm{Va}_m\mathrm{H}_n-\mathrm{Va/H}}^{b}$	0.29~1.53 eV

In CD model, several assumptions were employed (Li et al., 2012) as (a) the point defects executed a three-dimensional random walk, (b) only hydrogen and vacancies were mobile, the hydrogen-vacancy complexes were relatively immobile, (c) the nucleation of clusters proceeded via different types of reactions, including the formation, growth and dissociation of hydrogen-vacancy complexes, as well as the interactions of hydrogen and vacancies with dislocations and grain boundaries, respectively. In addition, both vacancy stabilization by hydrogen and vacancy absorption by dislocations and grain boundaries were included in the CD model. The primary reactions in CD model are present in Table 3. Based on these calculations, the concentration distribution of hydrogen-vacancy complexes along with cluster size and time were then obtained through numerical solution of a set of ordinary differential equations (ODEs) under different conditions, such as aging time, system temperature and inherent sinks (dislocation lines and grain boundaries).

Table 3 Reactions included in the CD model.

Va: vacancy, H: hydrogen, D: dislocation, G: grain boundary.

Reactions	Expression
Combination and decomposition of vacancies	$\mathrm{Va}_m + \mathrm{Va} \overset{E^b_{\mathrm{Va}_m-\mathrm{Va}}}{\leftrightarrow} \mathrm{Va}_{m+1}$
Combination and decomposition between $\mathrm{Va}_m\mathrm{H}_n$ and Va	$\mathrm{Va}_m\mathrm{H}_n + \mathrm{Va} \overset{E^b_{\mathrm{Va}_m\mathrm{H}_n-\mathrm{Va}}}{\leftrightarrow} \mathrm{Va}_{m+1}\mathrm{H}_n$
Combination and decomposition between $\mathrm{Va}_m\mathrm{H}_n$ and H	$\mathrm{Va}_m\mathrm{H}_n + \mathrm{H} \overset{E^b_{\mathrm{Va}_m\mathrm{H}_n-\mathrm{H}}}{\leftrightarrow} \mathrm{Va}_m\mathrm{H}_{n+1}$
Va absorption at dislocations	$\mathrm{D} + \mathrm{Va} \overset{E^b_{\mathrm{D+Va}}=\infty}{\rightarrow} \mathrm{DVa}$
H absorption and desorption in dislocations	$\mathrm{D} + \mathrm{H} \overset{E^b_{\mathrm{D+H}}}{\leftrightarrow} \mathrm{DH}$
Va absorption at grain boundaries	$\mathrm{G} + \mathrm{Va} \overset{E^b_{\mathrm{G+Va}}=\infty}{\rightarrow} \mathrm{GVa}$
H absorption at grain boundaries	$\mathrm{G} + \mathrm{H} \overset{E^b_{\mathrm{G+H}}=\infty}{\rightarrow} \mathrm{GH}$

Figure 8 shows the detailed size distribution functions (SDF) with the number of hydrogen and vacancies in a cluster at different aging times. We can clearly find that the size of nano-voids increases gradually with time during the long-time aging process. By summing all of the concentration of vacancies and hydrogen-vacancy complexes, the mean radius distribution of nano-voids at different times is further given in Fig. 9. We find that the size of the most probable cluster increases with time and is close to 0.37 nm at t = 100 s (see arrow indication in Fig. 9a), indicating that the excess vacancies tend to accumulate and a high-density of proto nano-voids can be formed. The size of 0.37 nm is on the same order to that observed in our early experiment (Neeraj et al., 2012). However, our simulations utilized a Va migration barrier of E_{Va}^{m} = 0.64 eV from theoretical calculations (Domain and Becquart, 2002; Ramasubramaniam et al., 2009), which is a little higher than that of 0.55 eV reported in experiments (Vehanen et al., 1982). To make our simulation more reasonable, we further performed the CD simulations by using the experimental value. The most probable size of cluster increases to about 0.70 nm at t = 100 s (see arrow indication in Fig. 9b) and is predicted to become even larger as time increases. The size is comparable to the depth of nano-voids detected on fracture surfaces experimentally (Neeraj et al., 2012). Further, when considering the effects of temperature, stress and stress triaxiality on promotion of nano-void formation, the cluster size might be even larger than predicted in the current simulations.

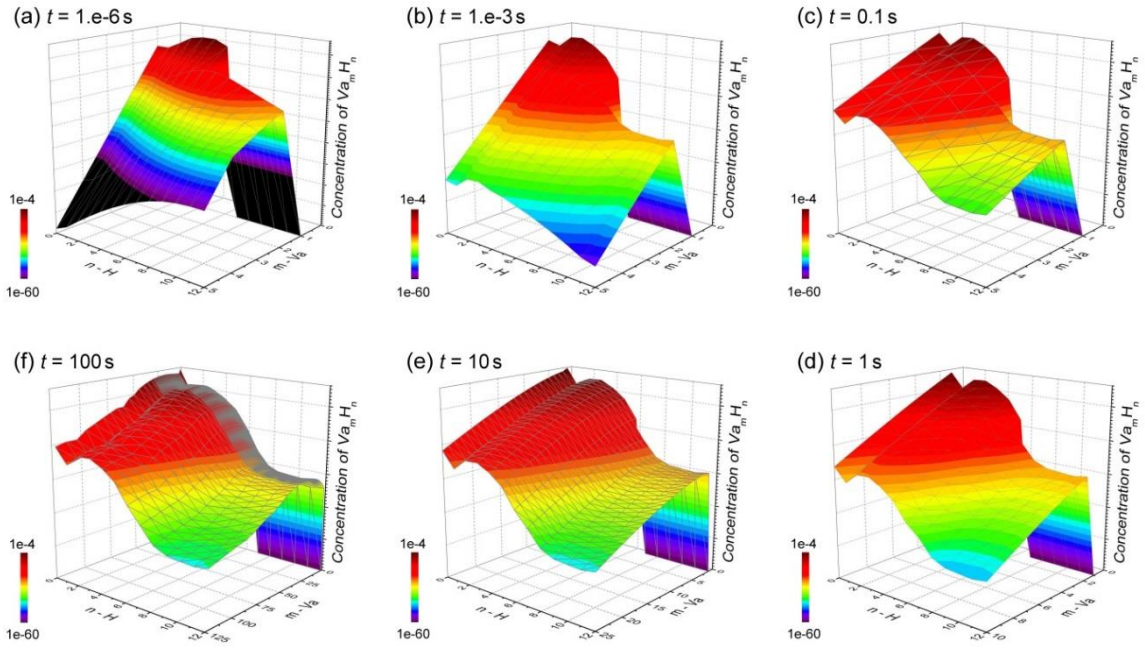

Fig. 8. (a)-(f) Size distribution function of nano-voids with the numbers of hydrogen and vacancies at different aging times.

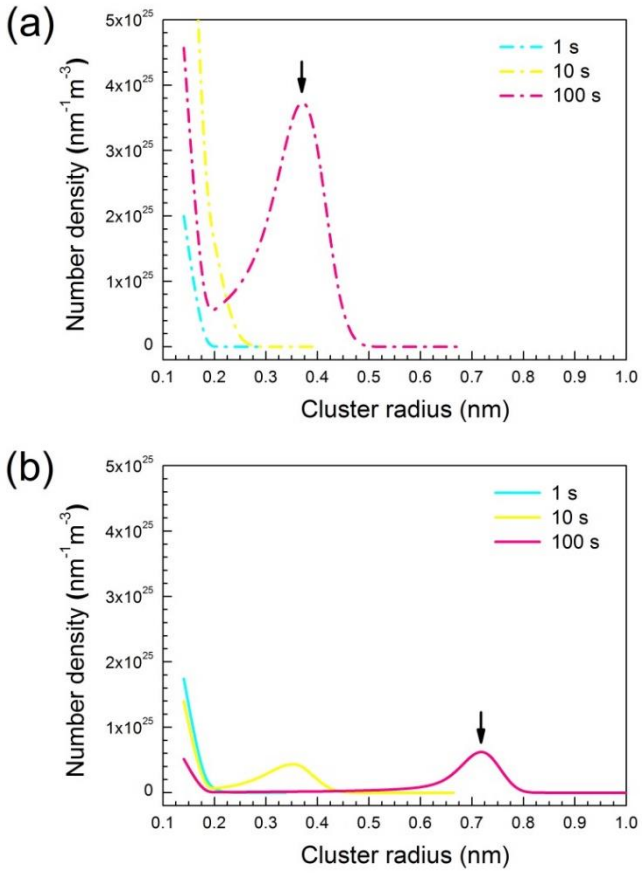

Fig. 9. Mean radius distributions of proto nano-voids at different aging times at room temperature by using CD simulations. (a) and (b) are the simulations results with E_{Va}^{m} = 0.64 eV in *ab initio* calculation (Domain and Becquart, 2002) and E_{Va}^{m} = 0.55 eV by experimental measurement (Vehanen et al., 1982), respectively. As time increases, the most probable size of cluster increases, indicating the accumulation of vacancies and hydrogen-vacancy complexes during long-time evolution.

Additionally, we should emphasize that current multi-scale simulations are focused on the nucleation stage of proto nano-voids in the context of hydrogen embrittlement when considering the proto nano-void radius is less than 1 nm. Based on our studies, we have shown that nano-void nucleation is governed by supersaturated vacancies generated in dislocation plasticity. The magnitude of C_{V} strongly relies on dislocation density. Since dislocation density is more related to shear flow stress, the present study on nano-voids nucleation in dislocation plasticity is more governed by shear stress. However, for the voids growth and coalescence, the stress triaxiality would take a crucial role (McClintock, 1968; Rice and Tracey, 1969).

3.4. Experimental evidence of hydrogen-vacancy complexes in literatures

In the following, we present recent experimental observations on H embrittlement that are consistent with the concept of hydrogen-vacancy complexes induced materials damage. We first show our experimental results and then present the evidence of hydrogen-vacancy complexes in literature. Finally, we present the implication of hydrogen-vacancy complexes on understanding the incipient microscopic damage of H embrittlement.

3.4.1. Experimental observations on nano-voids

Figure 10a is an example of the observation of significant dislocation plasticity during H embrittlement by transmission electron microscope (TEM). The thin foils for this study were prepared using focused ion beam (FIB) techniques and were extracted perpendicular to the fracture surface. The prepared foils contained the fracture surface and the observations were made right beneath the fracture surface to a few microns below the surface. Figure 10a shows deformation microstructure right beneath the fracture surface in a X65 sample tested in a tensile test with pre-charged H. The H content was measured to be about 1 wt. ppm diffusible H and 4 wt. ppm total H. In this sample the starting microstructure consisted of a ferrite grain size of 10 μm with subgrain size of 1-3 μm. After deformation in the presence of H the subgrain size was refined to 20-50 nm size observed in Fig. 10a. This indicates that extensive plastic deformation has caused significant grain refinement. While there will be some rearrangement of the dislocation structures when the crack passes through as well as from thin foil preparation, these changes are not significant to alter the essential conclusion that significant dislocation plasticity is associated with H embrittlement. Additional examples of evidence of significant crack-tip dislocation plasticity can be observed in the work of Neeraj et al (Neeraj et al., 2012) and these are consistent with other recent observations as well (Martin et al., 2011a; Martin et al., 2011b).

Figure 10b is an example of observation of nano-dimples on the quasi-brittle fracture surface of H embrittled samples by scanning electron microscopy (SEM). The sample was a line pipe grade X80 steel that was fractured in a 3000 psi (21MPa) high pressure H gas. These samples were tested in Sandia National Laboratories by Dr. Brian Somerday and were provided to the authors for microstructural study. Details of testing can be found in the publications by San Marchi et al (Marchi et al., 2010). The authors have also recently published a paper that provides additional experimental details and examples of deformation microstructure and fracture surface observation

(Neeraj et al., 2012). The topographical analysis by atomic force microscopy (AFM) along with high resolution SEM of the quasi-brittle fracture surfaces indicated that a high density of nano-dimples on the final fracture surface. The nano-dimples were the signature of failure during quasi-brittle fracture of H embrittlement (Neeraj et al., 2012). Based on the AFM and SEM data they have estimated the dimples to be about 5-20 nm wide but only about 1-5 nm deep. They have also performed conjugate surface analysis in the SEM to show that the two halves of the fracture surfaces contain matching dimples indicating they are two halves of nano-voids. Independent of the authors, Martin et al (Martin et al., 2011b) have also observed similar topographical features in the SEM and have also published an AFM image consistent with Neeraj et al's observations. Based on these observations a nano-void coalescence mechanism, induced by excess Va accumulation, has been proposed as the failure mechanism (Neeraj et al., 2012). Our multi-scale simulation work present above gives strong support to the experimental observations and bridges the link between atomic events and macroscopic damage.

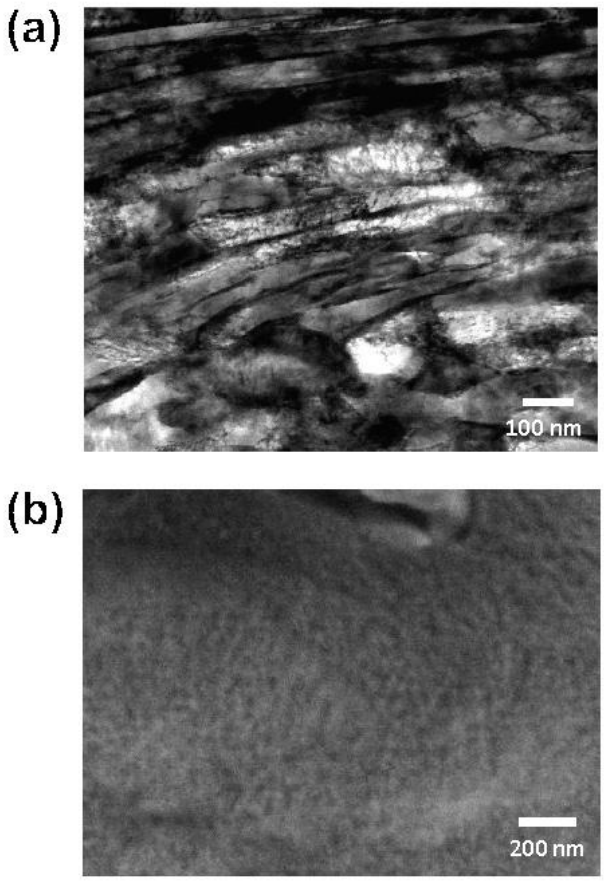

Fig. 10. Experimental observations on hydrogen embrittlement in steel. (a) TEM image of deformation microstructure underneath a hydrogen embrittled quasi-brittle fracture facet in a tensile tested X65 grade

linepipe steel. (b) SEM image of a typical hydrogen embrittled quasi-brittle fracture surface of X80 grade steel fracture toughness tested in 3000 PSI H_2 gas pressure.

3.4.2. The evidence of hydrogen-vacancy complexes in literatures

There are several experimental works that provide indirect evidence for hydrogen-vacancy complex formation and accumulation during plastic deformation. The observation of nano-scale dimples covering the entire fracture surface (Neeraj et al., 2012) implies that there was a very high nucleation of voids and very little growth during nano-void coalescence process. The hydrogen-vacancy complex would fit as the ideal candidate for rationalizing the experimental observation needing a very high density of void nucleation at the nano-scale. In the work of Takai et al (Takai et al., 2008), it was clearly shown that when "pure" iron and IN625 were deformed in the presence of H and were subsequently allowed to out gas the diffusible H and continue the deformation, the microstructural damage (and loss of ductility) persisted as if the material was continuously deformed in the presence of H. They report loss of ductility of about 25% in pure iron and over 90% in IN625 in the presence of H induced damage. Takai et al (Takai et al., 2008) have identified hydrogen-vacancy complexes as the cause for microstructural damage that was observed in their work. Sakaki et al (Sakaki et al., 2006) performed positron annihilation spectroscopy (PAS) to analyze the defect population after deforming iron in the presence and absence of H. They have concluded that deforming iron in the presence of H increased the accumulation of vacancies and generated vacancy clusters based on positron lifetime analysis. More recently, Doshida et al (Doshida et al., 2012) performed thermal desorption spectroscopy (TDS) and PAS analysis on H charged quenched and tempered martensitic steels. They observed that the mean positron lifetime increased towards the fracture surface in a statically loaded tensile test. They have also concluded that local deformation in the presence of H led to accumulation of excess vacancies and vacancy clusters and is the primary cause of microstructural damage. This accumulation was shown to increase and peak at the fracture surface as one approached from the interior towards the fracture surface. Further, fracture in this case was observed to be intergranular and Doshida et al have suggested that this is due to the hydrogen-vacancy complexes. In another work on martensitic steels, Doshida et al cyclically pre-deformed samples before performing monotonic tensile testing (Doshida et al., 2013). In this work they used H as tracer probe to indirectly characterize the presence of hydrogen-vacancy complexes. It was shown that cyclic deformation in the presence of H lead to generation of hydrogen-vacancy complexes that led to embrittlement during

subsequent monotonic tensile testing. Oudriss et al (Oudriss et al., 2012) have performed careful TDS in combination with characterization studies on pure nickel to show excess vacancy accumulation at grain boundaries in the presence of H which indicate that the hydrogen-vacancy complexes could play a role even in intergranular failure at grain boundaries (Oudriss et al., 2012). Finally, Hatano et al (Hatano et al., 2014) have performed TDS and PAS studies in austenitic stainless and have shown that the hydrogen-vacancy complexes are the root cause for the embrittlement observed when tensile tested in the presence of H in fcc austenitic materials. Therefore, there has been significant recent accumulation of indirect experimental evidence in the literature that the hydrogen-vacancy complexes play a critical role in material failure.

3.4.3. Implication of hydrogen-vacancy complexes on hydrogen-induced failure

Based on our simulations results and experimental evidence, we may expect the following consequences that the hydrogen-vacancy complexes take in the context of hydrogen-induced material failure. For those regions of stress-concentration such as a crack tip, the segregation of H can enhance localized dislocation plasticity as illustrated in HELP mechanism (Birnbaum and Sofronis, 1994; Robertson, 2001). Such strong dislocation plasticity can result in the generation of large amount of vacancies. In the presence of moderately enhanced local H concentration at crack tip regions, the vacancies are naturally stabilized by H to VaH_n complexes into a superabundant concentration. Such superabundant vacancy state has been supported by recent calculations (Hayward and Fu, 2013; Sugimoto and Fukai, 2014) and experimental measurements (Hatano et al., 2014). Since the vacancies are produced by dislocation processes, the VaH_n complexes are expected to be distributed near the slip planes and regions of dislocation plasticity. During continued damage evolution, the VaH_n complexes grow larger by Va accumulation through both displacive and diffusive processes to form proto nano-voids. This further leads to macroscopic failure by void growth and coalescence processes, which are consistent with experimental evidence for nano-voiding in hydrogen embrittled steels along quasi-brittle fracture surfaces (Martin et al., 2011a; Neeraj et al., 2012).

4. Conclusions

In summary, by using multi-scale simulations, we studied the basic properties of hydrogen-vacancy complex and revealed its role on proto nano-voids formation upon plastic deformation in α-Fe. Our atomistic calculations show that the hydrogen-vacancy complex has a good thermal

stability and low diffusivity. Different from vacancy, the hydrogen-vacancy complex even keep stable when meeting dislocation sinks. Our large-scale molecular dynamics simulations show that the dislocation motion and dislocation-dislocation intersections will produce a large amount of hydrogen-vacancy complexes when α-Fe is deformed at room temperature under H concentration of around 10^{-4}~10^{-2}. This can boost the Va concentration to a magnitude of 10^{3} within a computational supercell. Further, the cluster dynamics simulations show that during long-time evolution, the randomly distributed hydrogen-vacancy complexes prefer to grow in size by absorbing additional vacancies and act as nuclei for proto nano-voids. The current work bridges the link of hydrogen-vacancy complexes with the experimentally observed nano-voids upon plasticity in the presence of hydrogen. It might also help understanding the phenomenon on hydrogen-induced failure in iron and steels.

References

Ackland, G., Mendelev, M., Srolovitz, D., Han, S., Barashev, A., 2004. Development of an interatomic potential for phosphorus impurities in α-iron. J. Phys.: Condens. Matter 16, S2629.

Alinaghian, Y., Asadi, M., Weck, A., 2014. Effect of pre-strain and work hardening rate on void growth and coalescence in AA5052. Int. J. Plast. 53, 193-205.

Benzerga, A.A., Besson, J., Pineau, A., 2004. Anisotropic ductile fracture: Part II: theory. Acta Mater. 52, 4639-4650.

Birnbaum, H.K., Sofronis, P., 1994. Hydrogen-enhanced localized plasticity - a mechanism for hydrogen-related fracture. Mater. Sci. Eng. A 176, 191-202.

Brailsford, A.D., Bullough, R., 1972. The rate theory of swelling due to void growth in irradiated metals. J. Nucl. Mater. 44, 121-135.

Bringa, E.M., Traiviratana, S., Meyers, M.A., 2010. Void initiation in fcc metals: Effect of loading orientation and nanocrystalline effects. Acta Mater. 58, 4458-4477.

Daw, M.S., Baskes, M.I., 1984. Embedded-atom method - derivation and application to impurities, surfaces and other defects in metals. Phys. Rev. B 29, 6443-6453.

Domain, C., Becquart, C.S., 2002. Ab initio calculations of defects in Fe and dilute Fe-Cu alloys. Phys. Rev. B 65, 024103.

Doshida, T., Nakamura, M., Saito, H., Sawada, T., Takai, K., 2013. Hydrogen-enhanced lattice defect formation and hydrogen embrittlement of cyclically prestressed tempered martensitic steel. Acta Mater. 61, 7755-7766.

Doshida, T., Suzuki, H., Takai, K., Oshima, N., Hirade, T., 2012. Enhanced Lattice Defect Formation Associated with Hydrogen and Hydrogen Embrittlement under Elastic Stress of a Tempered Martensitic Steel. ISIJ Int. 52, 198-207.

Etienne, A., Hernandez-Mayoral, M., Genevois, C., Radiguet, B., Pareige, P., 2010. Dislocation loop evolution under ion irradiation in austenitic stainless steels. J. Nucl. Mater. 400, 56-63.

Fischer, F.D., Antretter, T., 2009. Deformation, stress state and thermodynamic force for a growing void in an elastic–plastic material. Int. J. Plast. 25, 1819-1832.

Fischer, F.D., Svoboda, J., Appel, F., Kozeschnik, E., 2011. Modeling of excess vacancy annihilation at different types of sinks. Acta Mater. 59, 3463-3472.

Fu, C.C., Dalla Torre, J., Willaime, F., Bocquet, J.L., Barbu, A., 2005. Multiscale modelling of defect kinetics in irradiated iron. Nature Mater. 4, 68-74.

Gangloff, R.P., Somerday, B.P., 2012. Gaseous Hydrogen Embrittlement of Materials in Energy Technologies: Mechanisms, modelling and future developments. Elsevier.

Gerberich, W.W., Oriani, R.A., Lii, M.J., Chen, X., Foecke, T., 1991. The necessity of both plasticity and brittleness in the fracture thresholds of iron. Philos. Mag. A 63, 363-376.

Golubov, S.I., Ovcharenko, A.M., Barashev, A.V., Singh, B.N., 2001. Grouping method for the approximate solution of a kinetic equation describing the evolution of point-defect clusters. Philos. Mag. A 81, 643-658.

Hardouin Duparc, A., Moingeon, C., Smetniansky-de-Grande, N., Barbu, A., 2002. Microstructure modelling of ferritic alloys under high flux 1 MeV electron irradiations. J. Nucl. Mater. 302, 143-155.

Hatano, M., Fujinami, M., Arai, K., Fujii, H., Nagumo, M., 2014. Hydrogen embrittlement of austenitic stainless steels revealed by deformation microstructures and strain-induced creation of vacancies. Acta Mater. 67, 342-353.

Hayward, E., Deo, C., 2011. Energetics of small hydrogen-vacancy clusters in bcc iron. J. Phys.: Condens. Matter 23, 425402.

Hayward, E., Fu, C.-C., 2013. Interplay between hydrogen and vacancies in α-Fe. Phys. Rev. B 87, 174103.

Henkelman, G., Uberuaga, B.P., Jonsson, H., 2000. A climbing image nudged elastic band method for finding saddle points and minimum energy paths. J. Chem. Phys. 113, 9901-9904.

Hirth, J.P., 1980. Effects of hydrogen on the properties of iron and steel. Metall. Trans. A 11, 861-890.

Hirth, J.P., Lothe, J., 1992. Theory of Dislocations, 2nd ed. Wiley, New York.

Hoover, W.G., 1985. Canonical dynamics: equilibrium phase-space distributions. Phys. Rev. A 31, 1695.

Iijima, Y., Kimura, K., Hirano, K., 1988. Self-diffusion and isotope effect in α-iron. Acta Metall. 36, 2811-2820.

Johnson, H.H., Morlet, J.G., Troiano, A.R., 1958. Hydrogen, crack initiation, and delayed failure in steel. Trans. Met. Soc. AIME 212, 528-536.

Khan, A.S., Liu, H., 2012. Strain rate and temperature dependent fracture criteria for isotropic and anisotropic metals. Int. J. Plast. 37, 1-15.

Kimizuka, H., Ogata, S., 2011. Slow diffusion of hydrogen at a screw dislocation core in alpha-iron. Phys. Rev. B 84, 024116.

Kiritani, M., 1973. Analysis of the clustering process of supersaturated lattice vacancies. J. Phys. Soc. Japan 35, 95-107.

Kraftmakher, Y., 1998. Equilibrium vacancies and thermophysical properties of metals. Phys. Rep. 299, 79-188.

Lau, T.T., Lin, X., Yip, S., Van Vliet, K.J., 2009. Atomistic examination of the unit processes and vacancy-dislocation interaction in dislocation climb. Scripta Mater. 60, 399-402.

Lecarme, L., Tekoglu, C., Pardoen, T., 2011. Void growth and coalescence in ductile solids with stage III and stage IV strain hardening. Int. J. Plast. 27, 1203-1223.

Li, H., Fu, M.W., Lu, J., Yang, H., 2011. Ductile fracture: Experiments and computations. Int. J. Plast. 27, 147-180.

Li, J., 2003. AtomEye: an efficient atomistic configuration viewer. Modell. Simul. Mater. Sci. Eng. 11, 173.

Li, Y.G., Zhou, W.H., Ning, R.H., Huang, L.F., Zeng, Z., Ju, X., 2012. A cluster dynamics model for accumulation of helium in tungsten under helium Ions and neutron irradiation. Commun. Comput. Phys. 11, 1547-1568.

Liu, Y.-L., Zhang, Y., Zhou, H.-B., Lu, G.-H., Liu, F., Luo, G.N., 2009. Vacancy trapping mechanism for hydrogen bubble formation in metal. Phys. Rev. B 79, 172103.

Lou, Y., Yoon, J.W., Huh, H., 2014. Modeling of shear ductile fracture considering a changeable cut-off value for stress triaxiality. Int. J. Plast. 54, 56-80.

Lu, G., Kaxiras, E., 2005. Hydrogen embrittlement of aluminum: The crucial role of vacancies. Phys. Rev. Lett. 94, 155501.

Malcher, L., Andrade Pires, F.M., César de Sá, J.M.A., 2014. An extended GTN model for ductile fracture under high and low stress triaxiality. Int. J. Plast. 54, 193-228.

Marchi, C.S., Somerday, B.P., Nibur, K.A., Stalheim, D.G., Boggess, T., Jansto, S., 2010. Fracture and fatigue of commercial grade API pipeline steels in gaseous hydrogen. Proceedings of the ASME Pressure Vessels and Piping Conference, Bellevue, WA, 939-948.

Martin, M.L., Fenske, J.A., Liu, G.S., Sofronis, P., Robertson, I.M., 2011a. On the formation and nature of quasi-cleavage fracture surfaces in hydrogen embrittled steels. Acta Mater. 59, 1601-1606.

Martin, M.L., Robertson, I.M., Sofronis, P., 2011b. Interpreting hydrogen-induced fracture surfaces in terms of deformation processes: A new approach. Acta Mater. 59, 3680-3687.

McClintock, F.A., 1968. A criterion for ductile fracture by the growth of holes. J. Appl. Mech. 35, 363-371.

Mecking, H., Estrin, Y., 1980. The effect of vacancy generation of plastic-deformation. Scripta Mater. 14, 815-819.

Meslin, E., Barbu, A., Boulanger, L., Radiguet, B., Pareige, P., Arakawa, K., Fu, C.C., 2008. Cluster-dynamics modelling of defects in α-iron under cascade damage conditions. J. Nucl. Mater. 382, 190-196.

Militzer, M., Sun, W.P., Jonas, J.J., 1994. Modeling the effect of deformation-induced vacancies on segregation and precipitation. Acta Metall. 42, 133-141.

Nagumo, M., Nakamura, M., Takai, K., 2001. Hydrogen thermal desorption relevant to delayed-fracture susceptibility of high-strength steels. Metall. Mater. Trans. A 32, 339-347.

Neeraj, T., Srinivasan, R., Li, J., 2012. Hydrogen embrittlement of ferritic steels: Observations on deformation microstructure, nanoscale dimples and failure by nanovoiding. Acta Mater. 60, 5160-5171.

Nose, S., 1984. A unified formulation of the constant temperature molecular-dynamics methods. J. Chem. Phys. 81, 511-519.

Ohsawa, K., Eguchi, K., Watanabe, H., Yamaguchi, M., Yagi, M., 2012. Configuration and binding energy of multiple hydrogen atoms trapped in monovacancy in bcc transition metals. Phys. Rev. B 85, 094102.

Oudriss, A., Creus, J., Bouhattate, J., Conforto, E., Berziou, C., Savall, C., Feaugas, X., 2012. Grain size and grain-boundary effects on diffusion and trapping of hydrogen in pure nickel. Acta Mater. 60, 6814-6828.

Plimpton, S., 1995. Fast parallel algorithms for short-range molecular-dynamics. J. Comput. Phys. 117, 1-19.

Ramasubramaniam, A., Itakura, M., Carter, E.A., 2009. Interatomic potentials for hydrogen in alpha-iron based on density functional theory. Phys. Rev. B 79, 174101.

Rice, J.R., Tracey, D.M., 1969. On the ductile enlargement of voids in triaxial stress fields∗. J. Mech. Phys. Solids 17, 201-217.

Robertson, I.M., 2001. The effect of hydrogen on dislocation dynamics. Eng. Fract. Mech. 68, 671-692.

Sakaki, K., Kawase, T., Hirato, M., Mizuno, M., Araki, H., Shirai, Y., Nagumo, M., 2006. The effect of hydrogen on vacancy generation in iron by plastic deformation. Scripta Mater. 55, 1031-1034.

Sofronis, P., McMeeking, R.M., 1989. Numerical analysis of hydrogen transport near a blunting crack tip. J. Mech. Phys. Solids 37, 317-350.

Song, J., Curtin, W.A., 2012. Atomic mechanism and prediction of hydrogen embrittlement in iron. Nature Mater. 12, 145-151.

Sugimoto, H., Fukai, Y., 2014. Hydrogen-induced superabundant vacancy formation in bcc Fe: Monte Carlo simulation. Acta Mater. 67, 418-429.

Takai, K., Shoda, H., Suzuki, H., Nagumo, M., 2008. Lattice defects dominating hydrogen-related failure of metals. Acta Mater. 56, 5158-5167.

Tasan, C.C., Hoefnagels, J.P.M., Diehl, M., Yan, D., Roters, F., Raabe, D., 2014. Strain localization and damage in dual phase steels investigated by coupled in-situ deformation experiments and crystal plasticity simulations. Int. J. Plast. 63, 198-210.

Tateyama, Y., Ohno, T., 2003. Stability and clusterization of hydrogen-vacancy complexes in alpha-Fe: An ab initio study. Phys. Rev. B 67, 174105.

Taylor, G.I., 1934. The mechanism of plastic deformation of crystals. Part I. Theoretical. Proc. Roy. Soc. London A 145, 362-387.

Taylor, G.I., 1938. Plastic strain in metals. J. Inst. Metals 62, 307–324.

Traiviratana, S., Bringa, E.M., Benson, D.J., Meyers, M.A., 2008. Void growth in metals: Atomistic calculations. Acta Mater. 56, 3874-3886.

Troiano, A.R., 1960. The role of hydrogen and other interstitials in the mechanical behavior of metals. Trans. ASM 52, 54-80.

Tutyshkin, N., Müller, W.H., Wille, R., Zapara, M., 2014. Strain-induced damage of metals under large plastic deformation: Theoretical framework and experiments. Int. J. Plast. 59, 133-151.

Valiev, R.Z., Ivanisenko, Y.V., Rauch, E.F., Baudelet, B., 1996. Structure and deformaton behaviour of Armco iron subjected to severe plastic deformation. Acta Mater. 44, 4705-4712.

Vehanen, A., Hautojarvi, P., Johansson, J., Ylikauppila, J., Moser, P., 1982. Vacancies and carbon impurities in alpha-iron: Electron-irradation. Phys. Rev. B 25, 762-780.

Xu, Z.T., Peng, L.F., Fu, M.W., Lai, X.M., 2015. Size effect affected formability of sheet metals in micro/meso scale plastic deformation: Experiment and modeling. Int. J. Plast. 68, 34-54.

Zehetbauer, M., 1993. Cold work-hardening in stage-IV and stage-V of fcc metals. 2. Model fits and physical results. Acta Metall. 41, 589-599.
Zhao, K.J., Chen, C.Q., Shen, Y.P., Lu, T.J., 2009. Molecular dynamics study on the nano-void growth in face-centered cubic single crystal copper. Comput. Mater. Sci. 46, 749-754.

Acknowledgements

J.L., S.L. Y.-C.L. and L.Q. acknowledge supports by NSF DMR-1240933 and DMR-1120901 and ExxonMobil Research and Engineering Company. Computational time on the Extreme Science and Engineering Discovery Environment (XSEDE) under the grant number TG-DMR130038 is gratefully acknowledged. X.D. and J.S. appreciate the support of NSFC (51171140, 51231008, 51321003), the 973 Programs of China (2010CB631003, 2012CB619402) and 111 project (B06025). T.N. and R.S. thank for the support of ExxonMobil Research and Engineering Company. S.L. and P.G. appreciate the support by Alexander von Humboldt Foundation. E. Hayward is thanked for providing the published data.